Emergent spatial patterns of competing benthic and pelagic algae in a river network: A parsimonious basin-scale modeling analysis

Soohyun Yang [a,b,*], Enrico Bertuzzo [c], Olaf Büttner [a], Dietrich Borchardt [a], P. Suresh C. Rao [b,d]

[a] Department of Aquatic Ecosystem Analysis and Management, Helmholtz Centre for Environmental Research-UFZ, 39114 Magdeburg, Germany
[b] Lyles School of Civil Engineering, Purdue University, West Lafayette, IN 47907, USA
[c] Dipartimento di Scienze Ambientali, Informatica e Statistica, Università Ca' Foscari Venezia, 30172 Venezia-Mestre, Italy
[d] Agronomy Department, Purdue University, West Lafayette, IN 47907, USA

ARTICLE INFO

ABSTRACT

Algae, as primary producers in riverine ecosystems, are found in two distinct habitats: benthic and pelagic algae typically prevalent in shallow/small and deep/large streams, respectively. Over an entire river continuum, spatiotemporal patterns of the two algal communities reflect specificity in habitat preference determined by geomorphic structure, hydroclimatic controls, and spatiotemporal heterogeneity in nutrient loads from point- and diffuse-sources. By representing these complex interactions between geomorphic, hydrologic, geochemical, and ecological processes, we present here a new river-network-scale dynamic model (C^nANDY) for pelagic (A) and benthic (B) algae competing for energy and one limiting nutrient (phosphorus, P). We used the urbanized Weser River Basin in Germany (7th-order; ~8.4 million population; ~46 K km^2) as a case study and analyzed simulations for equilibrium mass and concentrations under steady median river discharge. We also examined P, A, and B spatial patterns in four sub-basins. We found an emerging pattern characterized by scaling of P and A concentrations over stream-order ω, whereas B concentration was described by three distinct phases. Furthermore, an abrupt algal regime shift occurred in intermediate streams from B dominance in $\omega \leq 3$ to exclusive A presence in $\omega \geq 6$. Modeled and long-term basin-scale monitored dissolved P concentrations matched well for $\omega > 4$, and with overlapping ranges in $\omega < 3$. Power-spectral analyses for the equilibrium P, A, and B mass distributions along hydrological flow paths showed stronger clustering compared to geomorphological attributes, and longer spatial autocorrelation distance for A compared to B. We discuss the implications of our findings for advancing hydro-ecological concepts, guiding monitoring, informing management of water quality, restoring aquatic habitat, and extending C^nANDY model to other river basins.

1. Introduction

Algae are primary producers in streams and rivers, and are used as indicators to assess water quality and ecological status (Allan and Castillo, 2007; Stevenson and Smol, 2015). Identifying potential hot-spots for eutrophication (pelagic and benthic algal blooms) in impaired aquatic ecosystems resulting from anthropogenic pressures is key for mitigation and restoration (Le Moal et al., 2019). However, at the scale of an entire river network, this task is challenging as convolution along all flow paths is required to discern longitudinal patterns of pelagic and benthic algal communities, as hypothesized by the River Continuum Concept (Vannote et al., 1980). Such challenges are mainly attributed to the spatial heterogeneity and temporal dynamics in dominant coupled processes. Complex feedbacks among land-use patterns generating point- and diffuse-sources of nutrients, geomorphic attributes of the river network structure, hydrologic conditions (discharge and water stage), and geochemical dynamics (in-stream processes) combine to shape the ecological (algal) dynamics across river networks (Dong et al., 2017).

It is noteworthy that most efforts to develop process-based models of algal dynamics in rivers have focused only on pelagic algal community. Existing models cover a single river reach, such as RIVERSTRAHLER (Billen et al., 1994; Aissa-Grouz et al., 2018) and QSIM (Schöl et al., 1999), as well as the entire river network, such as TAPIR (Istvánovics et al., 2014), QUAL-NET (Minaudo et al., 2018), and the ANN-based model (Soro et al., 2020). Process-based

* Corresponding author.
  E-mail address: soohyun.yang@ufz.de (S. Yang).

models of coupled pelagic-benthic algal dynamics have been proposed (Pelletier et al., 2006; Jäger et al., 2017; Jäger and Borchardt, 2018), however their application has so far been restricted to a single reach. To our knowledge and available review papers [e.g., Sharma and Kansal (2013)], WASP7 is the only comprehensive, process-based model simulating both pelagic and benthic algal dynamics with coupled carbon-nitrogen-phosphorus processes using a mass-balance framework over entire river networks (Ambrose and Wool, 2009).

However, most process-based, complex models for simulating algal dynamics in river networks require extensive amount of observed data and/or estimates for fitting or calibrating model parameters (Flipo et al., 2004). Model simulations for a selected small study area typically match observed data only after thorough calibration of many model parameters (Hipsey et al., 2020). It is highly challenging to apply complex models at meso–scales or in data-poor river basins because of the daunting task of collecting and characterizing data, or because of the sparse availability of observational data caused by extensive resources needed for systematic, long-term monitoring campaigns over the whole catchment (Mannina and Viviani, 2010; Rutherford Christopher et al., 2020), particularly in developing countries (Chapra, 2011). Given these limitations and over-parameterization problems (Wellen et al., 2015), there is an increasing awareness of the need for simpler, process-based approaches in modeling river water quality and aquatic ecosystems by emphasizing holistic system understanding and for screening purposes (Kirchner, 2006; Jackson-Blake and Starrfelt, 2015). Embracing this spirit, a process-based parsimonious model for algal dynamics under steady-state river systems was developed (Chapra et al., 2014), but only for benthic algal community and at the scale of a single reach.

Parsimonious, but process-based, models for both pelagic and benthic algae at the whole river network scale inevitably face two key challenges in data-model comparisons: (1) uncertainty in parameter estimation, and (2) sparsity in observational data for model validation. Time-series data are often available at a single location (e.g., basin outlet) or synoptic sampling at multiple locations but at infrequent intervals. A possible alternative can be reliance on spatial analysis approaches for identifying spatial patterns of water quality and ecological status with the potential for transferring to other basins Yang et al., 2019a. In this spirit, we develop a river-network-scale parsimonious model, named *C^{n}ANDY* (Coupled Complex Algal-Nutrient Dynamics, Fig. 1A, Section 2.1), for simulating the coupled dynamics of pelagic and benthic algae competing for one limiting nutrient (phosphorus, P) and energy (solar radiation). We link, at the river-network-scale, the following key processes: (1) variability in water stage and discharge across all streams; (2) heterogeneity of point- and diffuse-sources of P; (3) in-stream geochemical processes for P cycling (hyporheic uptake); and (4) two dominant controls (nutrient and light) driving competitive growth of pelagic and benthic algae. Our modeling analyses can contribute to informing action plans for protection of river water quality and aquatic ecosystems to manage eutrophication, such as demanded by the EU Water Framework Directive (European Commission, 2000) and the United Nations Resolution on Global Water Quality (UNEP/JRC, 2019).

Our analyses of a river-basin-wide case study (Weser River in Germany, details in Section 2.2) are interpreted to test two primary hypotheses: one related to spatial patterns of the competing algal communities over the entire river network, and the other related to scaling of nutrient and algal patterns across the river network hierarchy. The River Continuum Concept (Vannote et al., 1980) and the process-based, reach-scale model simulations (Jäger et al., 2017; Jäger and Borchardt, 2018) suggest a longitudinal gradient from benthic algae dominance in upstream, shallow streams to pelagic algae prevalence in deeper, downstream reaches. We hypothesize that spatial patterns of pelagic and benthic algae would exhibit distinct, mutually exclusive, but predictable regimes across the river network, with shifts between pelagic and benthic algal regimes occurring wherever light penetration is significantly limited by the river stage and pelagic algal shading.

Universally consistent scaling signatures exist within river network structure (Dodds and Rothman, 2000; Rodríguez-Iturbe and Rinaldo, 2001; Yang and Paik, 2017), and are reflected also in scaling of hydraulic geometry (Leopold and Maddock, 1953; Dong et al., 2019), geochemical attributes (Basu et al., 2011; Bertuzzo et al., 2017), human settlement patterns (Fang et al., 2018; Yang et al., 2019a), and anthropogenic pressures descriptors (Miyamoto et al., 2011; Yang et al., 2019b). On this basis, we hypothesize that ecological metrics (e.g., algal biomass, gross algal primary production) would also exhibit similar scaling features.

2. Methods and materials

2.1. C^{n}ANDY model structure

For each reach i with a length l_i, two types of algal habitats exist: a streambed with a width w_i, and a surface water column with a depth d_i (from the surface to the streambed). We assume one algal taxon that can grow in both benthic and pelagic habitats such as species of the genera *Navicula, Dinobryon, Scenedesmus* (Jäger et al., 2017; Jäger and Borchardt, 2018), relying on needed nutrients and light resources. Algal dynamics are coupled with macro- and micro-nutrients in reality, however, in the spirit of a parsimonious approach discussed before, we consider only nutrient phosphorus, which is known to be the key limiting nutrient for algal growth in many fresh waters, and to often trigger eutrophication (Carpenter, 2008; Aissa-Grouz et al., 2018; Liang et al., 2020) We assume vertically well-mixed dissolved P within a reach, equally available for both pelagic and benthic algae. Hence, one state variable for dissolved inorganic phosphorus (P, in the units of mass) is coupled with state variables for benthic and pelagic algae (B and A, respectively in the mass units) based on a mass balance approach.

In each river reach, we assume steady-state water flow with a constant mean velocity v_i that transports both the dissolved nutrient and the pelagic algae. Based on a single reach model developed for the coupled dynamics of phosphorus and two competing algae (Jäger et al., 2017; Jäger and Borchardt, 2018), we describe the temporal dynamics of the three state variables for every reach (P_i, B_i, and A_i) in our network model as:

$$\frac{dP_i}{dt} = \phi_{i,WWTP} + \phi_{i,DS} + \sum_j E_j \frac{Q_j P_j}{V_j} - \frac{Q_i P_i}{V_i}$$
$$- cG_{B,i}B_i - cG_{A,i}A_i - \frac{v_{f,i}}{d_i}P_i \tag{1}$$

$$\frac{dB_i}{dt} = G_{B,i}B_i - \mu_{L,B}B_i - \mu_s B_i \tag{2}$$

$$\frac{dA_i}{dt} = G_{A,i}A_i - \mu_{L,A}A_i + \mu_s B_i + \sum_j E_j \frac{Q_j A_j}{V_j} - \frac{Q_i A_i}{V_i}. \tag{3}$$

Symbols, definitions, and the associated units for all state variables and parameters are defined in **Table S1 in the Supplementary Information (SI)**. The input loads of nutrient phosphorus in reach i consist of three types: (1) discharges from wastewater treatment plants, WWTPs (as $\phi_{i,WWTP}$, point-source loads), (2) delivered from direct drainage areas categorized by different land covers (as $\phi_{i,DS}$, diffuse-source loads), and (3) transported from all upstream reaches j (as $\sum_j E_j Q_j P_j/V_j$, where E_j is an element of the connectivity matrix marking river flow existence (i.e., $E_i=1$, $E_i=0$ if no flow exists) between the upstream reach j and the down-

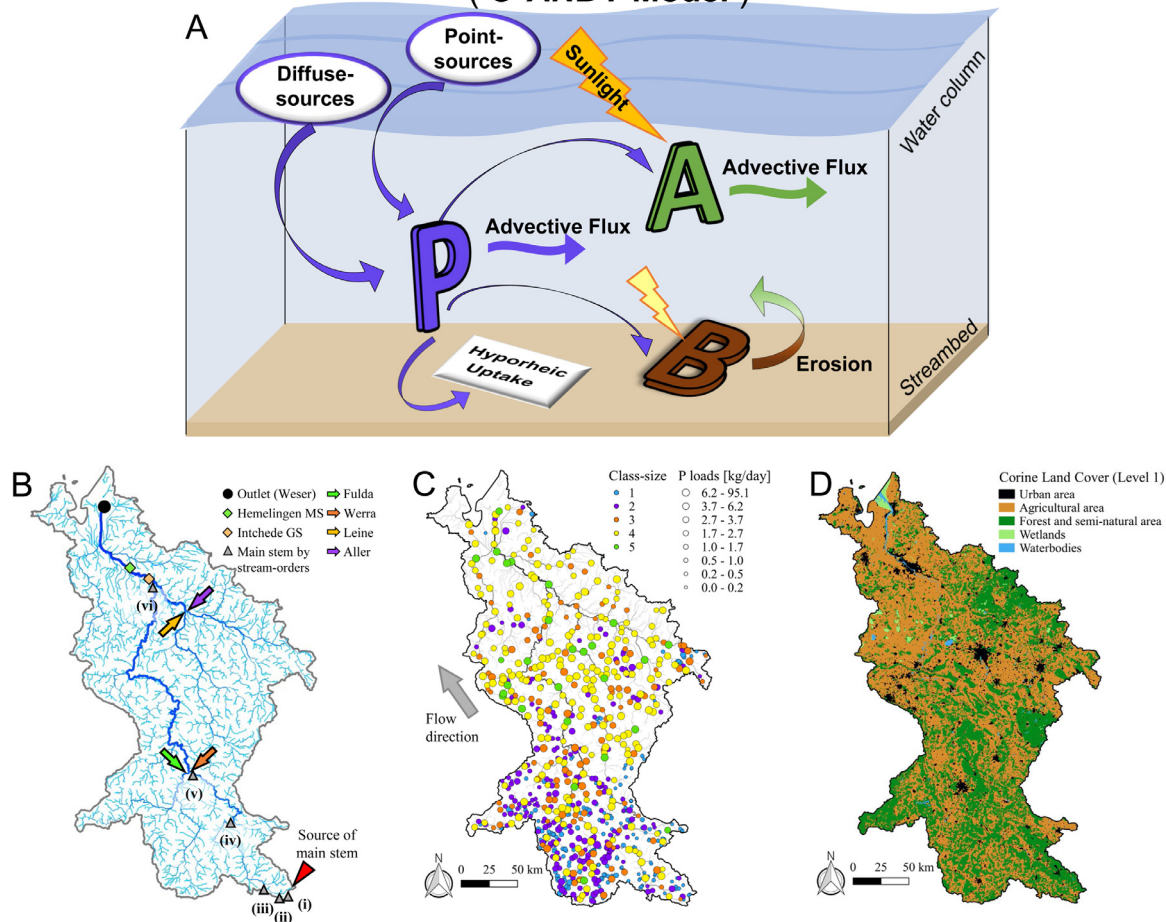# Coupled, Complex Algal-Nutrient DYnamics
(C^nANDY Model)

Fig. 1. Introduction of the C^nANDY model and the Weser River Basin. **(A)** Schematic representation of processes among nutrient phosphorus (P), pelagic (A) and benthic algae (B) for a given stream reach in the C^nANDY model. **(B)** Weser River Network. Along the main stem, the most downstream points by stream orders from 1 to 7 are marked (gray triangles). Arrows show confluences of four main sub-basins converging into the 5th stream-order (Fulda, Werre, Leine, and Aller). **(C)** Spatial distribution of point-source P loads from WWTPs with five class-sizes (color-coded) and magnitude of P loads discharged (circle-sized). **(D)** Spatial patterns of five types of land cover delivering diffuse-source nutrient loads. (For interpretation of the references to colour in this figure legend, the reader is referred to the web version of this article.)

stream reach i, and Q_j is river discharge and V_j is of the volume of the upstream reach j). We assume that both $\phi_{i,WWTP}$ and $\phi_{i,DS}$ are temporally invariant for each reach i. The advection mechanism leads to the output flux of the dissolved nutrient for the reach i (as Q_iP_i/V_i). Moreover, the dissolved nutrient phosphorus in reach i is removed by two key processes: (1) nutrient uptake by both benthic and pelagic algae in reach i to contribute to gross primary production for both algal communities assuming a constant algal nutrient to carbon quota c (as $c(G_{B,i}B_i + G_{A,i}A_i)$, where $G_{B,i}$ and $G_{A,i}$ are the growth rate of benthic and pelagic algae, respectively), and (2) natural attenuation through hyporheic zone of which the net uptake rate is inversely related to the depth d (as $v_{f,i}/d_i$, where $v_{f,i}$ is the uptake velocity for phosphorus in the hyporheic zone) (Basu et al., 2011). In this study, we assume spatially homogeneous v_f as 0.17 m/day estimated from our former study (Yang et al., 2019b). We implicitly consider abiotic processes for P into the first-order decay term by assuming a net sink effect for each reach. Regeneration of P in the water column through recycling of dead algae is not explicitly expressed in the model processes, because it would be of minor importance when compared to anthropogenic nutrient P loads from point- and diffuse-sources in urbanized and cultivated catchments. The decisions were based on the goal to develop a parsimonious approach that considers the first-order (dominant) processes and sources.

New algal biomass is produced at gross production rate $G_{B,i}$ on the streambed, and at $G_{A,i}$ in the water column of reach i. Existing algae in the benthic and pelagic habitats of reach i are lost at the rate of $\mu_{L,B}$ and $\mu_{L,A}$, respectively. Here, we assume that grazing effects in each habit dominantly contribute to the loss rates. Due to scouring effect, benthic algae suffer additional loss at rate μ_s. The detached benthic algae emigrate to the water column and, in turn, are involved in pelagic algae biomass. Advective flux for pelagic algae is embedded in the temporal dynamics of pelagic algae in reach i, which are the influx from direct upstream reaches and the outflux at the reach i downstream.

The gross production rate of benthic algae is related to the light intensity that penetrates on the streambed ($I_{d,i}$), the available nutrient, and the density effect with maximum concentration for benthic algae under neither light- nor nutrient limitations (B_K):

$$G_{B,i} = \mu_p \frac{I_{d,i}}{I_{d,i} + h} \frac{P_i}{P_i + mV_i} \left(1 - \frac{B_i}{B_K S_i}\right). \tag{4}$$

The light intensity is vertically attenuated by light-blocking of pelagic algae with an attenuation coefficient k and by background turbidity with coefficient k_{bg}. According to Lambert-Beer's law with light intensity on the top of water column (I_o), $I_{d,i}$ is

expressed as:

$$I_{d,i} = I_o \exp\left(-d_i\left(k\frac{A_i}{V_i} + k_{bg}\right)\right). \tag{5}$$

Following Huisman and Weissing (1995) and more recent works [e.g. Jäger and Borchardt (2018)] we assume that light and a single dissolved nutrient co-limit primary production of pelagic algae in reach i as:

$$G_{A,i}(I_i(d), P_i) = \mu_p \frac{I_i(d)}{I_i(d) + h}\frac{P_i}{P_i + mV_i} \tag{6}$$

where $I_i(d)$ is the light intensity that penetrates in reach i at depth d. Since vertically well-mixed water in reach i is assumed, pelagic algae production can be expressed (Huisman and Weissing, 1995) by averaging Eq. (6) over the water depth of reach i, d_i, as:

$$G_{A,i} = \mu_p \frac{1}{d_i(kA_i/V_i + k_{bg})} \ln\left(\frac{h + I_o}{h + I_{d,i}}\right)\frac{P_i}{P_i + mV_i}. \tag{7}$$

We ran the model under steady-state river discharge condition, spatially homogeneous light intensity at the water surface, and constant (but spatially variable) nutrient loads input. Seasonally variable shading from riparian vegetation, especially in small upstream reaches, and seasonal temperature variations were not considered in this model. Initial conditions were set as spatially homogeneous concentrations with 50 mgP/m^3 for dissolved phosphorus, 200 mgC/m^3 for pelagic algae, and 100 mgC/m^2 for benthic algae, being aligned with reference conditions. Boundary condition at the river basin outlet was considered as existing advective flux for nutrient and pelagic algae. We numerically integrated the model equations until the system reached the temporal equilibrium-state for all three state variables (all time derivative almost equal to zero). Specifically, we simulated the system through a forward explicit Euler scheme until, starting from the initial condition, steady-state was reached (the differences between two subsequent timesteps of every state variable are less than 10^{-6}). We used a daily timestep which always ensured convergence to the steady state solution. Note that the steady-state solution is independent of the initial condition, but an initial condition close to the steady-state solution can accelerate convergence. Mass and concentration at the equilibrium for a given variable Z ($Z = P$, A, and B) are denoted as Z* and Z*$_{conc}$, respectively.

We estimated depth (d_i) and width (w_i) for each reach i based on power-law scaling with river discharge (Q_i) for the same frequency of occurrence, well-known as downstream hydraulic geometry (Leopold and Maddock, 1953), as:

$$w_i = K_w Q_i^{\alpha_w} \tag{8}$$

$$d_i = K_d Q_i^{\alpha_d} \tag{9}$$

where the power-law exponents $\alpha_w = 0.5$ and $\alpha_d = 0.4$ are consistently found from many rivers (Leopold and Maddock, 1953; Knighton, 1998), and coefficients $K_w = 10$ [m$^{1-3\alpha_w}$s$^{-\alpha_w}$] and $K_d = 0.25$ [m$^{1-3\alpha_d}$s$^{-\alpha_d}$]. Since K_w and K_d are positively correlated (Knighton, 1998), we note that changing their values would insignificantly affect varying spatial patterns at a river-network-scale for the state variables at the equilibrium.

2.2. Study area

Our study area is Germany's largest national river basin, Weser River of ~46 K km^2 (Fig. 1B). The river network was extracted using 100 m x 100 m grid DEMs with a channel forming area of 10 km^2 (Zink et al., 2017). The delineated river network consists of ~1700 stream segments, here a segment means a channel portion between two successive confluences. The main stem (~700-km long) stretches from a small tributary in south-eastern part

to the basin outlet with the final 7th stream-order (Horton, 1945; Strahler, 1957). Small streams with low-orders from 1 to 3 account for ~86% of a total length of ~12 K km. Note that again our core interest is the river-network-scale spatial dynamics of the coupled P and two algal communities under a temporally representative hydrological condition. We considered steady-state median river discharge over the entire Weser River by multiplying drainage area of a given point within the river network with median value of specific discharge ($q = 203$ mm/yr) in May (1950–2019) measured at the Intschede gaging station shown in Fig. 1B. Spatial variability in hydroclimatic forcing is out of our scope here. Total phosphorus inputs to the Weser River are estimated as ~3440 tons P/yr, with 28% from point-sources and 72% from diffuse-sources. Essential descriptions for the point- and diffuse-sources and the monitoring data are given in below three sub-sections. Detailed information for the study area, such as hydrological conditions and P loads estimation by land covers, is described in SI-Sec. S1.

2.2.1. Point-sources of P

In the Weser River Basin, ~845 wastewater treatment plants (WWTPs) serving ~8.4 million people with ~97% connection (EEA, 2017) with a mean density of ~2 WWTPs/100 km^2, and a mean separate distance of ~11 km (Fig. 1C) were identified from national-scale reliable dataset for ~8900 WWTPs in Germany (Büttner, 2020). German WWTPs are categorized based on the magnitude serving population equivalent as five class-sizes, based on German regulations (https://www.gesetze-iminternet.de/abwv/anhang_1.html). Two largest class-sizes deploy the mandatory tertiary treatment technology to satisfy regulatory nutrient loads discharged, while the other three small class-sizes have no regulatory requirements (EEC, 1991). Around 957 tons P/yr loads for 2012–2016 are discharged to the Weser River from all WWTPs, and the two large class-sizes (~31% of total WWTPs) contribute to ~680 tons P/yr discharge (~ 71% of total). Larger class-sizes WWTPs are clustered toward the basin outlet, while smaller ones towards upstream (Yang et al., 2019a).

2.2.2. Diffuse-sources of P

Land cover patterns in the Weser River Basin were based on the CORINE Land Cover (CLC) 100 m grid data version 20 for 2012 year to be consistent with point-source loads data reference time (https://land.copernicus.eu/pan-european/corine-land-cover). The CLC spatial map for the Weser River Basin (Fig. 1D) manifests the dominance of agricultural areas (~59%), the scattered urban areas (~9%), and upstream clustered formation of forest/semi-natural areas (~31%).

2.2.3. Archived monitoring data

The scope of available monitoring dataset aligned with this study should be stressed: (1) only pelagic chlorophyll-a concentration during March to October (2000–2018) at the Hemelingen station which is located most downstream without tidal effect shown in Fig. 1B (SKUMS, 2019); (2) orthophosphate as phosphorus and total phosphorus concentrations during January to December (2000–2018) at the Hemelingen station (BfG, 2019); and (3) soluble reactive phosphorus (SRP) concentration at ~300 locations covering all 7 stream-orders, obtained from the official EIONET (European Environmental Information and Observation Network) and WFD sample sites. We used the first two dataset for estimating key model parameters (details in SI-Sec.S2), and the last one for our model validation to maximize the available data application (given in Section 3.2).

2.3. Data analysis metrics

Spatial pattern analyses were implemented through two primary aspects: (1) the spatial hierarchy by stream-orders (ω) in

a river network or by the associated contributing drainage areas that comprehensively characterize geomorphic features in a given river basin, and (2) the power spectral to quantify the patterns of the longitudinal distributions of our interested variables along flow paths. Detailed explanation and the associated references are given in SI-Sec. S3.

3. Results and discussion

3.1. Spatial patterns of phosphorus and algal biomass

A^*_{conc} and B^*_{conc} exhibited opposite spatial trends. A^*_{conc} was higher in larger streams along the main stem Fig. 2A), while B^*_{conc} was higher in small headwater streams (Fig. 2B). These results are aligned with well-known habitat preferences (Hilton et al., 2006; Jäger and Borchardt, 2018), indicating that our model formulation and simulations generate essential aspects of the drivers for growth of the two algae competing for light and nutrient (SI-Fig. S1). The contrasting patterns between A^*_{conc} and B^*_{conc} result from three factors: (1) benthic algae outcompete pelagic algae for available P in small streams, and lower river stage promotes sufficient light penetration; (2) pelagic algae dominate in larger streams, where light limitations from depth and pelagic algal shading combine to preclude benthic algae; and (3) higher density of pelagic algae limits growth by self-shading.

Given the lack of monitoring data for the network-scale algal concentrations within the network, to corroborate the simulated spatial patterns for A^*_{conc} and B^*_{conc}, we relied on the EU-scale authorized assessment status in 2016 for phytoplankton and macrophytes/phytobenthos for the Weser River Basin (European Environment Agency, 2018) (Figs. 2C and D), as the two indicators from four biological quality elements determining ecological status for surface water bodies under the EU WFD (European Commission, 2000). We stress that simulation results of a parsimonious model cannot be always demonstrated through empirical data [e.g., Chapra et al. (2014)]. In that case the relevant proxy can be used for indirect demonstration of parsimonious model results. Note that the color-coded status levels cannot directly be compared with the spatial gradients in A^*_{conc} and B^*_{conc}, because the status assessment criteria are based on taxonomic abundance and composition of the indicative parameters. Nevertheless, the referred maps (Figs. 2C and D) indirectly support the occurrence of pelagic algae mostly in large streams (Fig. 2A) and the prevalence of benthic algae in small streams (Fig. 2B), respectively. Despite cumulative input P loads, lower P^*_{conc} in larger streams resulted from combined losses via in-stream spiraling and algal uptake, while locally higher P^*_{conc} in smaller streams was mainly attributed to P loads from WWTPs (Fig. 2E). Mean of P^*_{conc} (148 mgP/m^3) over the entire Weser River exceeded by almost 50% the level needed to achieve *good* ecological status ($<$100 mgP/m^3 for Total P), as defined by the EU WFD (Heidecke et al., 2015).

Over stream-orders, distinct patterns for P^*_{conc}, A^*_{conc}, and B^*_{conc} emerged (Fig. 2F). Consistent changes for P^*_{conc} and A^*_{conc} over ω were, respectively, quantified using Hortonian scaling ratios of $R_{PC} = 1.43$ and $R_{AC} = 1.91$ ($R^2>0.9$, $p<0.01$). For B^*_{conc}, ω-based pattern was characterized by an inverse logistic curve as ω decreased, with three distinct phases: plateau, transitional, and absence. This emergent pattern for B^*_{conc} with lower coefficient of variation (CV) for smaller ω clearly represented consistently preferred habitats in small streams for benthic algae. Indeed, A^*_{conc} in $\omega >4$ and B^*_{conc} in $\omega <5$ were larger than their respective detectable concentrations, manifesting the mutual exclusivity in dominance regime for the two algal communities. Compared to the mutually exclusive zones, algal regime transitional zones in intermediate streams ($\omega = 4$~5) had 10~80% smaller gross primary production (GPP) estimated for the two algae (GPP$_{A+B}$) with higher

CV (Fig. 2G), because of abrupt transition from benthic to pelagic algae dominance (Fig. 2H). The algal regime shift is expected to be a general phenomenon across diverse river basins because of the distinct habitat preference between pelagic and benthic algae (Vannote et al., 1980; Jäger and Borchardt, 2018). However, since the algal regime shift is affected by multiple attributes of the river basins and algal traits, we cannot conclude that other river basins would show the same regime shift we reported here. Note that simulation results presented herein are based on the effects of best representative grazers for a given steady median river discharge (SI-Sec. S2). Role of grazers on the spatial patterns is presented in SI-Sec. S4 and Figs. S2-S3.

3.2. Comparisons to phosphorus long-term monitoring data

For $\omega \leq 3$, the range of SRP concentrations monitored in May during 2000–2015 period (Fig. 3A) and the corresponding simulated values of P^*_{conc} overlapped, but the median values were about two times different at the 1% significance level (Kruskal-Wallis test), (Figs. 3B, C, and D). In contrast, for the higher-order streams ($\omega \geq 4$), there were no significant differences between the two distributions (Figs. 3B, E and F). The discrepancy for small streams is attributable to non-concurrent sampling times and intervals over the 16 year monitoring. Furthermore, small streams with low-orders are the most heterogeneous in terms of hydrologic, biogeochemical and ecological conditions, and have variations in light intensity and temperature at monitoring times. On the other hand, the simulated P^*_{conc} were based on spatial homogeneity in environmental factors and constant median discharge. Nevertheless, data-model match in $\omega \geq 4$ suggests the pronounced effects of converging river flows and accumulated nutrient loads towards downstream to reduce the impacts of spatial heterogeneities (McGuire et al., 2014).

3.3. Heterogeneity among four sub-basins

Spatial heterogeneity of diffuse- and point-sources P loads across the Weser River Basin contributed to variabilities in P^*_{conc}, A^*_{conc}, and B^*_{conc} in four sub-basins (Fulda, Werra, Leine, and Aller) (see Fig 1B; SI-Table S2). Using the empirical probability density functions (pdfs) and their statistical moments, Weser River sub-basins were placed in two groups for P^*_{conc}, A^*_{conc}, and B^*_{conc}, but for different reasons (SI-Fig S4). Fulda and Werra were grouped for P^*_{conc} distributions because of their common patterns for more distributed point-source P loads from smaller WWTPs and lower magnitude of diffuse-source P loads per unit-area. Basin shape contributed to grouping Werra and Leine for A^*_{conc} because continuous, longer main stem in these more elongated sub-basins is favorable habitat of pelagic algae. For B^*_{conc}, Aller sub-basin was distinct from the others because larger number of smaller streams in this least elongated basin received directly larger point-source P loads (see Figs 1B and C; and SI-Table S2). Such differences in nutrient and algal spatial patterns would help understand likely outcomes in two large, urbanized international river basins (Elbe, Rhine) in Germany, and other EU basins. Intensive monitoring within one of the most representative sub-basins combined with fewer locations in the other three sub-basins of the Weser River Basin would be an option for optimizing limited resources for monitoring program establishment in future.

3.4. Spatial scaling along hydrologic flow paths

The geomorphic area-distance function, $D_G(x)$, (Fig. 4A) characterized the physical structure of the river network, with peaks in $D_G(x)$ reflecting the larger number of distal 1st-order streams in
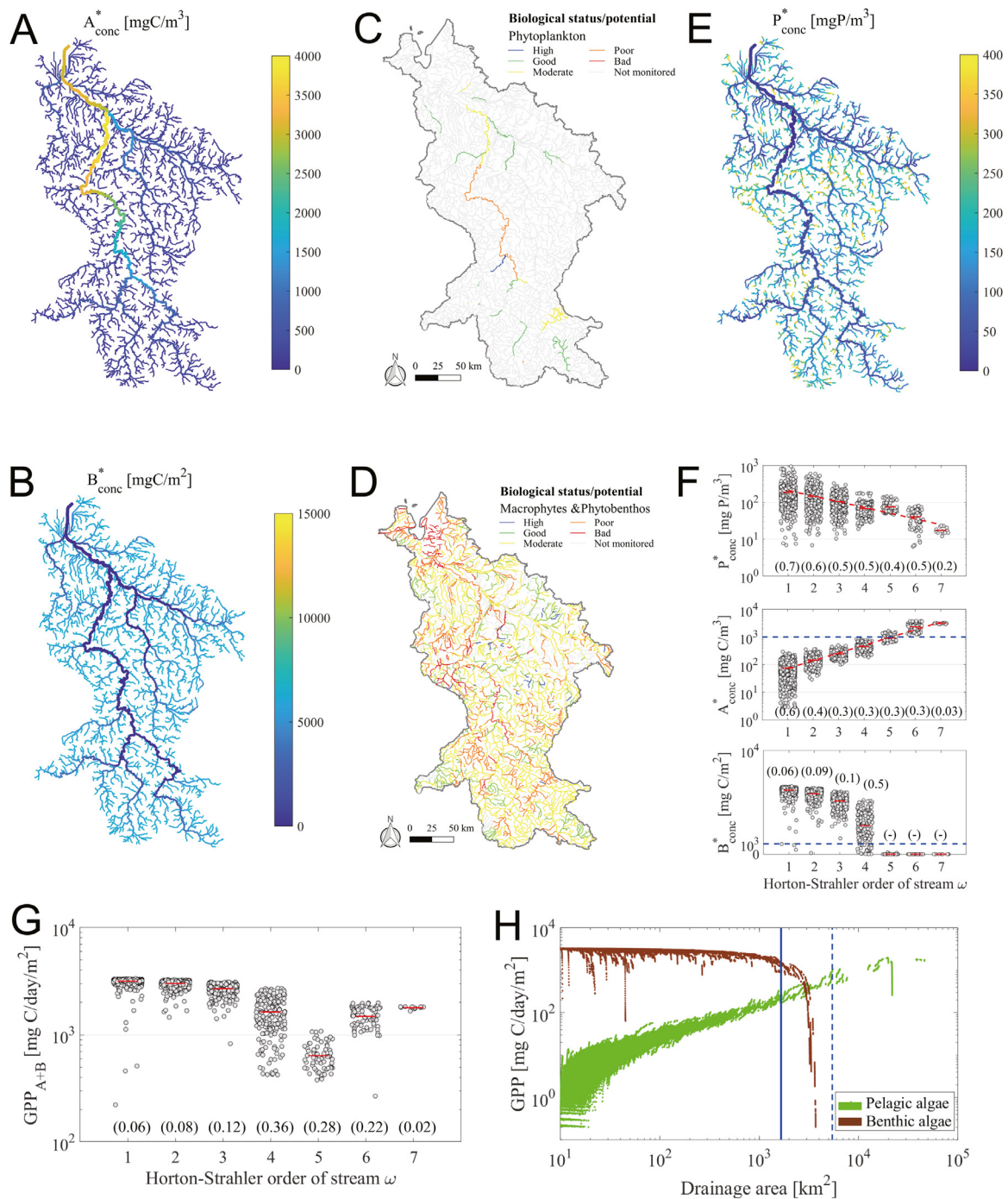
Fig. 2. Spatial patterns of the simulated results. (**A and B**) Distribution of the simulated equilibrium-state concentrations of pelagic (A^*_{conc}) and benthic (B^*_{conc}) algal biomass. (**C and D**) EU-scale authorized assessment on biological status/potential for phytoplankton and macrophytes/phytobenthos. (**E**) Distribution of the simulated equilibrium-state concentrations of dissolved P (P^*_{conc}). (**F**) Stream-order (ω) based distributions for P^*_{conc}, A^*_{conc}, and B^*_{conc}. Red dashed lines for P^*_{conc} and A^*_{conc} indicate Hortonian scaling for respective mean values (red bar). Blue dashed lines indicate detectable concentrations for each of A^*_{conc} and B^*_{conc}. Numbers in each parenthesis are the CV for the depicted results within the same ω. (note different scales). (**G**) Over ω, distribution of gross primary production for both algae biomass (GPP_{A+B}) with mean values (red bar) and the CV in each parenthesis. (**H**) GPP distribution for respective algae over drainage area. Transitional phase between solid and dashed blue lines (mean drainage area of ω=4th and 5th, respectively) demonstrates the discontinuity in Fig. 2G. (For interpretation of the references to colour in this figure legend, the reader is referred to the web version of this article.)

the dendritic branching network. Compared to $D_G(x)$, both the geo-chemical distance function for the simulated equilibrium P mass (P^*), $D_{P^*}(x)$ (Fig. 4B), and the distance function for the simulated equilibrium pelagic algae mass (A^*), $D_{A^*}(x)$ (Fig. 4C), were more skewed towards the basin outlet ($\Psi_{P^*} = 0.9$; $\Psi_{A^*} = 0.5$). Overall, the magnitude of spatial fluctuations in $D_{P^*}(x)$ and $D_{A^*}(x)$ increased towards the basin outlet. These findings reflect the higher cumula-

tive P and A mass in larger streams (core of the main stem) than in smaller streams (merging tributaries). Interestingly, the distance function for the simulated equilibrium benthic algal mass (B^*), $D_{B^*}(x)$ (Fig. 4D), showed not only similar skewness ($\Psi_{B^*} = 1.0$) but also almost identical shape with $D_G(x)$. Such coincidence resulted from small streams serving as the preferred habitats for benthic algae. Thus, $D_G(x)$ serves as an excellent indicator for benthic algal
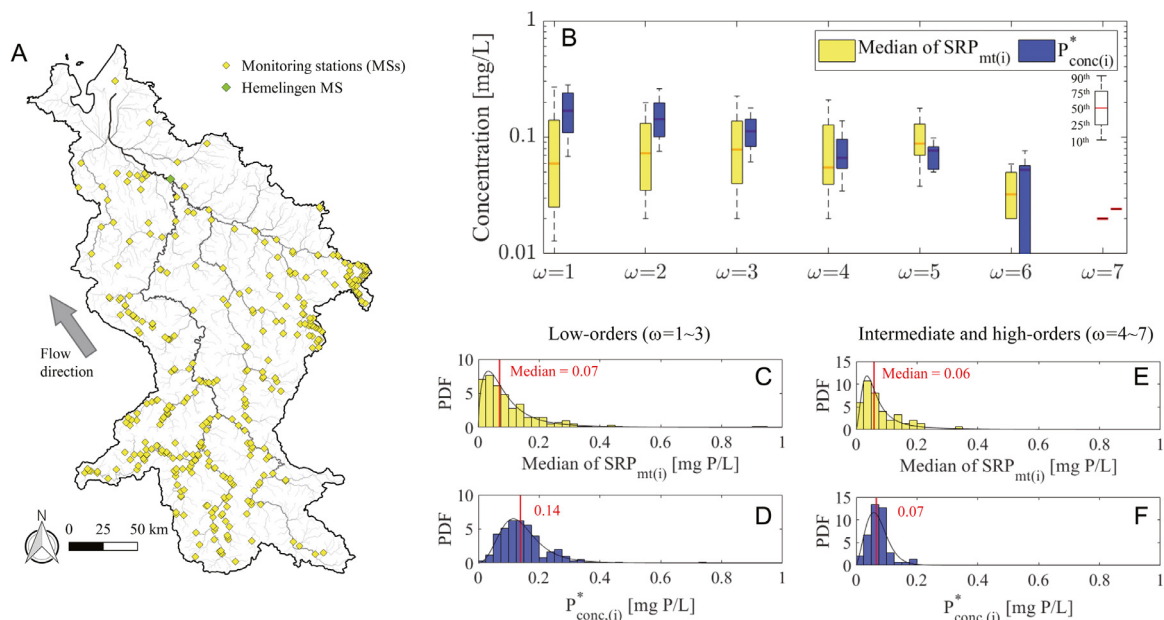
Fig. 3. Comparison between monitored data for SRP and the simulated equilibrium P*$_{conc}$. **(A)** Map for ~300 monitoring stations of which SRP data are available in May for 2000–2015. **(B)** By stream-orders ($\omega = 1\text{~}7$), comparison between median concentration of the monitored SRP data at a station i (SRP$_{mt(i)}$) located in a given ω and the P*$_{conc}$ at the corresponding location of the station i in the model domain (P*$_{conc(i)}$). **(C-F)** Comparison between normalized distributions (pdf type) of median SRP$_{mt(i)}$ (yellow) and P*$_{conc(i)}$ (blue): **(C-D)** for low-order streams ($\omega = 1\text{~}3$) and **(E-F)** for intermediate- and high-order streams ($\omega = 4\text{~}7$). Each black line indicates the best-fitted pdf (Burr Type VII distribution) at the 1% significance level (Kolmogorov-Smirnov test). (For interpretation of the references to colour in this figure legend, the reader is referred to the web version of this article.)
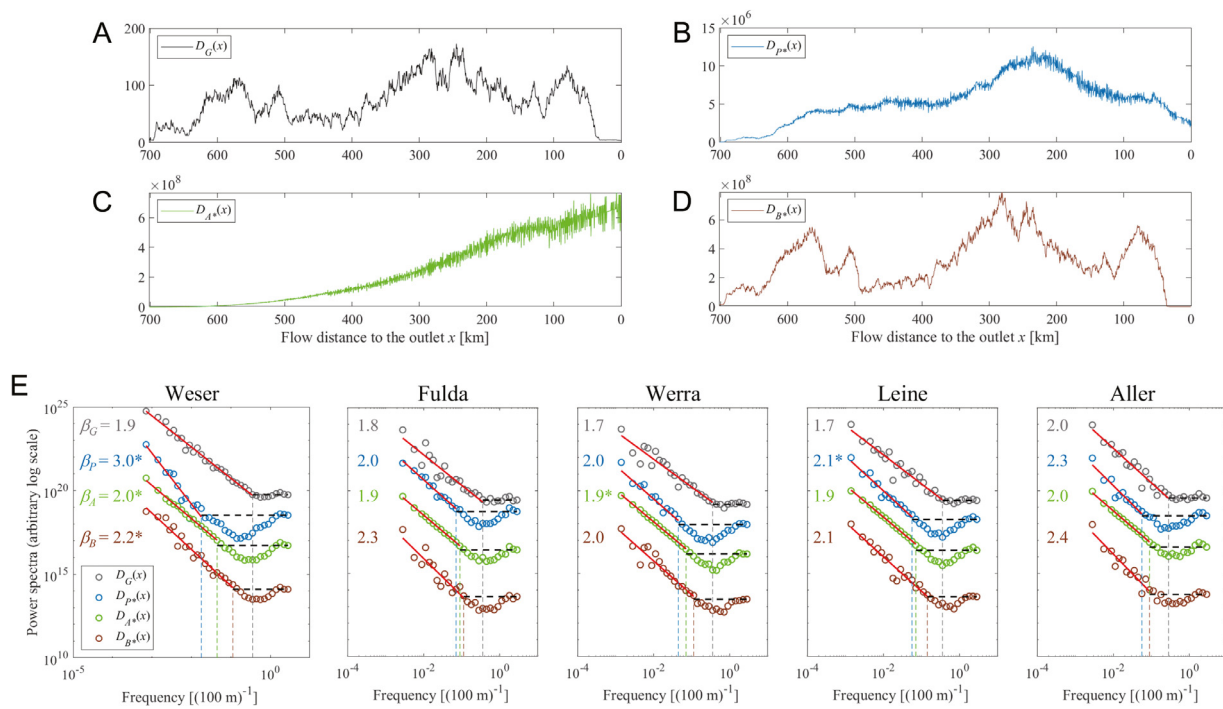

Fig. 4. Distance functions and the associated power spectral analysis. **(A, B, C, and D)** Distance functions for the Weser River show 1-D representation of spatial variations in geomorphology ($D_G(x)$), simulated equilibrium mass of dissolved phosphorous ($D_{P^*}(x)$), pelagic algae ($D_{A^*}(x)$), and benthic algae ($D_{B^*}(x)$). **(E)** Corresponding power-spectra on a log-log plot and their power-law slopes (β_z), and frequency thresholds (f^*) where there is a break from inverse to a line with zero slope. All power-law slopes are significant ($R^2 > 0.9$, $p < 0.01$). Significantly different slopes ($p < 0.01$) from β_G are marked with asterisk. (For interpretation of the references to colour in this figure legend, the reader is referred to the web version of this article.)

biomass distribution in a river basin, if P concentrations are above the thresholds required to support algal growth.

In the Weser River Basin and its four sub-basins, power-spectral analyses for all distance functions showed a distinct bi-fractal pattern (Fig. 4E). Power-law fits in spectral plots (slopes β_G, β_P, β_A, and β_B in Fig. 4E) were significant for all four sub-basins and the

entire Weser River Basin ($R^2 > 0.84$, $p < 0.01$). The values of β_G (1.7–2.0) had consistent spectral slopes (1.2–2.1) resulting from fractal river network structure (Marani et al., 1994; Fang et al., 2018). For the Weser River, the spectral slope β_G was significantly lower than all the other three exponents (an average of 2.4) ($p < 0.01$), indicating stronger spatial autocorrelation in $D_{P^*}(x)$, $D_{A^*}(x)$ and $D_{B^*}(x)$

than $D_G(x)$. Accordingly, P*, A*, and B* were more clustered in the longitudinal direction. Indeed, degree of their clustering was ~60% larger than clustering of population in the Weser River Basin (no city with >5 M inhabitants) (Yang et al., 2019a), suggesting stronger effects of environmental controls on the coupled P and algae than on pattern of urban settlements.

Threshold frequency (f^*) differentiating between the spatial autocorrelation signal and no-memory (i.e., zero slope) was the highest for $D_G(x)$, meaning the least interference of random-noise in $D_G(x)$. On average ~40% smaller f^* values for $D_{A*}(x)$ than those for $D_{B*}(x)$ indicated longer distance required to manifest spatial autocorrelation for pelagic algae. The behavior of pelagic and benthic algae may be compared to fish and benthic macroinvertebrates, respectively, based on underlying similarity in rivers, i.e., transport (floating/moving) along flows vs. static (attached/crawling) on stream bottom. More than eight times longer spatial autocorrelation distance for fish than that for benthic macroinvertebrates (Lloyd et al., 2006; Grenouillet et al., 2008) supports the feasibility of our findings. Moreover, β_B was ~12% higher than β_A (at 5% confidence level) indicates stronger clustering in the distribution of B* than A*.

3.5. Limitations and potential applications of C^nANDY model

We acknowledge that the C^nANDY model needs further improvement to reflect a wider range of environmental conditions and controls. We need to expand the current model framework to transient flows driven by seasonal and intra-annual variations in stochastic hydroclimatic forcing. We will further explore alternative approaches to estimate statistical distributions of the state variables for each reach of interest. We do not consider spatial heterogeneities in benthic habitat conditions associated benthic algal coverage in small streams, and hydrodynamic variabilities and shading from riparian vegetation, which produce nonuniform patterns of pelagic algae coverage in larger streams. The effects of spatial and temporal variations in temperature are also not considered in our modeling.

Nevertheless, the simulations we present provide an improved understanding of the complex-drivers for the emergent spatial patterns of competing pelagic and benthic algae at the river-network-scale. Spatially variable nutrient (P) loads and steady river discharge reflect landscape attributes (e.g., spatial patterns of human settlements) and hydroclimatic drivers (e.g., median discharge based on landscape filtering of precipitation). Moreover, the general framework of the C^nANDY model can be used for simulating nutrient and algal responses in other large urbanized river basins, by extending our earlier work on scaling of urban settlements and (surrogate) P loads in Rhine and Elbe River Basins (Yang et al., 2019a). Extensions to other river basins is also feasible, as are specific scenario-based simulations to inform targeted management strategies and to understand climate change impacts on eutrophication.

3.6. Ecological and management implications

In the Weser River, most small streams ($\omega \leq 3$) are projected to be dominated by large biomass of benthic algae, thus compromising the integrity of aquatic habitats supporting high biological diversity (Besemer et al., 2013; Baattrup-Pedersen et al., 2018). Targeted approaches to reduce P loads, both from point- and diffuse-sources, are required to improve water quality and ecological status of these most numerous and important streams (Büttner et al., 2020), although remarkable ~70% reduction of total P loads input was achieved over the past few decades (SI-Fig. S5). Management choices include upgrading some of the small WWTPs serving larger communities to advanced treatment technologies; how-

ever, installing such centralized upgraded wastewater treatment systems is an expensive option. Alternatively, deploying nature-inspired nutrient treatment (e.g., constructed wetlands) in conjunction with current primary and secondary wastewater treatment (Bolton et al., 2019) may be a cost-effective option. Pelagic algae are likely to be prevalent in larger streams ($\omega > 5$) in the Weser River network which compromise various ecosystem services along the river and in the estuary. Restoration of larger, deep river reaches is confronted by challenges of large flow volumes (high discharge). Various engineered structures (e.g., dams), flow-diversions, and engineered drainage of croplands have all changed geomorphic features and hydrologic dynamics of the river networks and play a major role in deteriorating water quality and ecological status of the entire river network (Palmer and Ruhi, 2019).

Projecting climate change impacts requires an understanding of dramatic shifts in extreme hydrologic events with associated geochemical and ecological alterations in river networks (Mosley, 2015). Increased flow variabilities (intense floods, extended droughts) and land-use changes have already caused widespread adverse impacts in river basins in Germany (Reinermann et al., 2019), rest of the EU (Buras et al., 2020), and elsewhere in the world (Michalak, 2016). Accordingly, the algal regime shifts we noted for steady discharge, are likely to vary in time under transient-flow conditions resulting from stochastic hydroclimatic forcing at daily scales, and seasonality in river hydrologic regimes (Xia et al., 2020). The algal regime transition zones we identified here from C^nANDY model simulations are likely to shift downstream during persistent drought conditions, when median river discharge and stage are significantly lower [e.g., as low as 100 m³/s, as observed during persistent heatwaves and droughts in Germany during May-Nov. for 2018 – 2019; (BfG, 2019)], and upstream during high-discharge and water stage during spring floods. Furthermore, increased duration and magnitude of droughts will lead to more intense benthic dominance in a larger fraction of the river network, while increased frequency of larger floods will contribute to stripping of benthic algal mats, and export of pelagic algae farther downstream, with implications to receiving surface waters (lakes, estuaries).

4. Conclusions

We presented a new river-network-scale model (C^nANDY) to simulate coupled pelagic-benthic algae and nutrient spatial dynamics, driven by competition for limiting nutrient (P) and energy (light). The salient contribution of the C^nANDY model was to deploy parsimonious descriptions for complex hydrologic-geochemical-ecological processes over the entire river network, facilitating investigation of both pelagic and benthic algal responses to spatially heterogeneous nutrient inputs from point- and diffuse-sources. Our model simulations under steady median river discharge for Germany's largest national river network (Weser River) showed mutual exclusivity between pelagic and benthic algae dominance, aligned with well-known contrasting habitat preference of the two algae (large/deep streams for pelagic and small/shallow ones for benthic). Our simulated concentrations for pelagic and benthic algae were consistent with the available ecological data, and those for phosphorus corresponded surprisingly well with the long-term nutrient monitoring data over the river basin.

The novel elements of our study were the emergent spatial patterns for the biomass and concentrations of benthic and pelagic algae, and phosphorus concentration over the large river network with heterogeneous point- and diffuse-sources of phosphorus. Stream-order based consistent scaling characterized the concentrations of pelagic algae and phosphorus. Algal regime shift from benthic to pelagic algae dominance was reveled in intermediate-

order streams, mainly attributed to the change of river network geometry and the associated hydrologic conditions. Longitudinal spatial scaling features for algal biomass related to their spatial autocorrelations were identified across the Weser River Basin and within four sub-basins. Future efforts will focus on incorporating spatially heterogeneous and dynamic conditions, including transient river discharge and impacts of seasonal changes in temperature and riparian shading. High-spatial resolution algal monitoring data are needed for further validation of modeling analyses, and these have to cover benthic and pelagic habitats consistently. The model results may inform respective monitoring designs. The general C^nANDY model may also support the advancement of mechanistic hydro-ecological concepts and theory regarding environmental processes and controls in aquatic ecosystems, and are useful for guiding future water quality monitoring and management efforts to mitigate/prevent eutrophication in anthropogenically impacted large river basins.

Declaration of Competing Interest

The authors declare that they have no known competing financial interests or personal relationships that could have appeared to influence the work reported in this paper.

Acknowledgments

Supplementary materials

Supplementary material associated with this article can be found, in the online version, at doi:10.1016/j.watres.2021.116887.

References

Aissa-Grouz, N., Garnier, J., Billen, G., 2018. Long trend reduction of phosphorus wastewater loading in the Seine: determination of phosphorus speciation and sorption for modeling algal growth. Environ. Sci. Pollut. R. 25 (24), 23515–23528.

Allan, J.D., Castillo, M.M., 2007. Stream Ecology: Structure and Function of Running Waters, 2nd ed. Springer, Dordrecht.

Ambrose, R.B., Wool, T.A., 2009. WASP7 Stream transport Model Theory and User's guide: Supplement to Water Quality Analysis Simulation Program (WASP) User Documentation. Environmental Protection Agency, Athens, GA, USA Retrieved from https://cfpub.epa.gov/si/si_public_record_report.cfm?Lab=NERL&dirEntryId=213988.

Büttner, O., 2020. DE-WWTP-data Collection of Wastewater Treatment Plants of Germany (Status 2015, Metadata). HydroShare.

Büttner, O., Jawitz, J.W., Borchardt, D., 2020. Ecological status of river networks: stream order-dependent impacts of agricultural and urban pressures across ecoregions. Environ. Res. Lett. 15 (10), 1040b1043.

Baattrup-Pedersen, A., Larsen, S.E., Andersen, D.K., Jepsen, N., Nielsen, J., Rasmussen, J.J., 2018. Headwater streams in the EU Water Framework Directive: evidence-based decision support to select streams for river basin management plans. Sci. Total Environ. 613-614, 1048–1054.

Basu, N.B., Rao, P.S.C., Thompson, S.E., Loukinova, N.V., Donner, S.D., Ye, S., Sivapalan, M, 2011. Spatiotemporal averaging of in-stream solute removal dynamics. Water Resour. Res. (10) 47.

Bertuzzo, E., Helton, A.M., Hall, R.O., Battin, T.J., 2017. Scaling of dissolved organic carbon removal in river networks. Adv. Water Resour. 110, 136–146.

Besemer, K., Singer, G., Quince, C., Bertuzzo, E., Sloan, W., Battin, T.J., 2013. Headwaters are critical reservoirs of microbial diversity for fluvial networks. Proc. R. Soc. B 280 (1771), 20131760.

BfG. (2019). Water levels – data from selected gauging stations on German federal waterways and shipping administration (WSV). Available from the German federal institute of hydrology (Bundesanstalt für Gewässerkunde) https://www.bafg.de/EN/06_Info_Service/01_WaterLevels/waterlevels.html.

Billen, G., Garnier, J., Hanset, P., 1994. Modelling phytoplankton development in whole drainage networks: the RIVERSTRAHLER model applied to the Seine river system. Hydrobiologia 289 (1), 119–137.

Bolton, L., Joseph, S., Greenway, M., Donne, S., Munroe, P., Marjo, C.E., 2019. Phosphorus adsorption onto an enriched biochar substrate in constructed wetlands treating wastewater. Ecol. Eng. X 1, 100005.

Buras, A., Rammig, A., Zang, C.S., 2020. Quantifying impacts of the 2018 drought on European ecosystems in comparison to 2003. Biogeosciences 17 (6), 1655–1672.

Carpenter, S.R., 2008. Phosphorus control is critical to mitigating eutrophication. Proc. Natl. Acad. Sci. U.S.A. 105 (32), 11039.

Chapra, S.C., 2011. Rubbish, Stink, and Death: the historical evolution, present state, and future direction of water-quality management and modeling. Environ. Eng. Res. 16 (3), 113–119.

Chapra, S.C., Flynn, K.F., Christopher Rutherford, J., 2014. Parsimonious model for assessing nutrient impacts on periphyton-dominated streams. J. Environ. Eng. 140 (6), 04014014.

Dodds, P.S., Rothman, D.H., 2000. Geometry of river networks. I. Scaling, fluctuations, and deviations. Phys. Rev. E 63 (1), 016115.

Dong, T.Y., Nittrouer, J.A., Czapiga, M.J., Ma, H., McElroy, B., Il'icheva, E., Pavlov, M., Chalov, S., Parker, G., 2019. Roles of bank material in setting bankfull hydraulic geometry as informed by the Selenga River Delta, Russia. Water Resour. Res. 55 (1), 827–846.

Dong, X., Ruhí, A., Grimm, N.B., 2017. Evidence for self-organization in determining spatial patterns of stream nutrients, despite primacy of the geomorphic template. Proc. Natl. Acad. Sci. U.S.A. 114 (24), E4744.

EEA, 2017. Urban Wast Water Treatment. European Environment Agency, Copenhagen, Denmark https://www.eea.europa.eu/data-and-maps/indicators/urban-waste-water-treatment/urban-waste-water-treatment-assessment-4.

EEC., 1991. Council directive of 21 May 1991 concerning urban waste water treatment (91/271/EEC). Off. J. Eur. Commun.. Retrieved from http://ec.europa.eu/environment/water/water-urbanwaste/index_en.html.

European Commission, 2000. Directive 2000/60/EC of the European parliament and of the council of 23 October 2000 establishing a framework for community action in the field of water policy. Off. J. Eur. Commun.. Retrieved from http://ec.europa.eu/environment/water/water-framework/index_en.html.

European Environment Agency, 2018. Quality Element Status. European Environment Agency, Copenhagen, Denmark https://www.eea.europa.eu/themes/water/european-waters/water-quality-and-water-assessment/water-assessments/quality-elements-of-water-bodies.

Fang, Y., Ceola, S., Paik, K., McGrath, G.S., Rao, P.S.C., Montanari, A., Jawitz, J.W, 2018. Globally universal fractal pattern of human settlements in river networks. Earth's Future 6.

Flipo, N., Even, S., Poulin, M., Tusseau-Vuillemin, M.-H., Ameziane, T., Dauta, A., 2004. Biogeochemical modelling at the river scale: plankton and periphyton dynamics: grand Morin case study. France. *Ecol. Model.* 176 (3), 333–347.

Grenouillet, G., Brosse, S., Tudesque, L., Lek, S., Baraillé, Y., Loot, G., 2008. Concordance among stream assemblages and spatial autocorrelation along a fragmented gradient. Divers. Distrib. 14 (4), 592–603.

Heidecke, C., Hirt, U., Kreins, P., Kuhr, P., Kunkel, R., Mahnkopf, J., Schott, M., Tetzlaff, B., Venohr, M., Wagner, A., Wendland, F., 2015. Endbericht zum Forschungsprojekt "Entwicklung eines Instrumentes für ein flussgebietsweites Nährstoffmanagement in der Flussgebietseinheit Weser. Thünen Report 21.

Hilton, J., O'Hare, M., Bowes, M.J., Jones, J.I., 2006. How green is my river? A new paradigm of eutrophication in rivers. Sci. Total Environ. 365 (1), 66–83.

Hipsey, M.R., Gal, G., Arhonditsis, G.B., Carey, C.C., Elliott, J.A., Frassl, M.A., Janse, J.H., de Mora, L, Robson, B.J., 2020. A system of metrics for the assessment and improvement of aquatic ecosystem models. Environ. Modell. Softw. 128, 104697.

Horton, R.E., 1945. Erosional development of streams and their drainage basins; hydrophysical approach to quantitative morphology. Geol. Soc. Am. Bull. 56 (3), 275–370.

Huisman, J., Weissing, F.J., 1995. Competition for nutrients and light in a mixed water column: a theoretical analysis. Am. Nat. 146 (4), 536–564.

Istvánovics, V., Honti, M., Kovács, Á., Kocsis, G., Stier, I., 2014. Phytoplankton growth in relation to network topology: time-averaged catchment-scale modelling in a large lowland river. Freshw. Biol. 59 (9), 1856–1871.

Jäger, C.G., Borchardt, D., 2018. Longitudinal patterns and response lengths of algae in riverine ecosystems: a model analysis emphasising benthic-pelagic interactions. J. Theor. Biol. 442, 66–78.

Jäger, C.G., Hagemann, J., Borchardt, D., 2017. Can nutrient pathways and biotic interactions control eutrophication in riverine ecosystems? Evidence from a model driven mesocosm experiment. Water Res 115, 162–171.

Jackson-Blake, L.A., Starrfelt, J., 2015. Do higher data frequency and Bayesian auto-calibration lead to better model calibration? Insights from an application of INCA-P, a process-based river phosphorus model. J. Hydrol. 527, 641–655.

Kirchner, J.W., 2006. Getting the right answers for the right reasons: linking measurements, analyses, and models to advance the science of hydrology. Water Resour. Res. 42 (3).

Knighton, D., 1998. Fluvial Forms and Processes. Edward Arnold, London.

Le Moal, M., Gascuel-Odoux, C., Ménesguen, A., Souchon, Y., Étrillard, C., Levain, A., Moatar, F., Pannard, A., Souchu, P., Lefebvre, A., Pinay, G, 2019. Eutrophication: a new wine in an old bottle? Sci. Total Environ. 651, 1–11.

Leopold, L.B., Maddock, T.J., 1953. The hydraulic geometry of stream channels and some physiographic implications. United States Geol. Surv. Prof. Pap. 252.

Liang, Z., Soranno, P.A., Wagner, T., 2020. The role of phosphorus and nitrogen on chlorophyll a: evidence from hundreds of lakes. Water Res. 185, 116236.

Lloyd, N.J., Nally, R.M., Lake, P.S., 2006. Spatial scale of autocorrelation of assemblages of benthic invertebrates in two upland rivers in south-eastern Australia and its implications for biomonitoring and impact assessment in streams. Environ. Monit. Assess. 115 (1), 69–85.

Mannina, G., Viviani, G., 2010. A parsimonious dynamic model for river water quality assessment. Water Sci. Technol. 61 (3), 607–618.

Marani, M., Rinaldo, A., Rigon, R., Rodriguez-Iturbe, I., 1994. Geomorphological width functions and the random cascade. Geophys. Res. Lett. 21 (19), 2123–2126.

McGuire, K.J., Torgersen, C.E., Likens, G.E., Buso, D.C., Lowe, W.H., Bailey, S.W., 2014. Network analysis reveals multiscale controls on streamwater chemistry. Proc. Natl. Acad. Sci. U.S.A. 111 (19), 7030.

Michalak, A.M., 2016. Study role of climate change in extreme threats to water quality. Nature 535, 349–350.

Minaudo, C., Curie, F., Jullian, Y., Gassama, N., Moatar, F., 2018. QUAL-NET, a high temporal-resolution eutrophication model for large hydrographic networks. Biogeosciences 15 (7), 2251–2269.

Miyamoto, H., Hashimoto, T., Michioku, K., 2011. Basin-wide distribution of land use and human population: stream order modeling and river basin classification in Japan. Environ. Manage. 47 (5), 885–898.

Mosley, L.M., 2015. Drought impacts on the water quality of freshwater systems; review and integration. Earth Sci. Rev. 140, 203–214.

Palmer, M., Ruhi, A., 2019. Linkages between flow regime, biota, and ecosystem processes: implications for river restoration. Science 365 (6459), eaaw2087.

Pelletier, G.J., Chapra, S.C., Tao, H., 2006. QUAL2Kw – A framework for modeling water quality in streams and rivers using a genetic algorithm for calibration. Environ. Modell. Softw. 21 (3), 419–425.

Reinermann, S., Gessner, U., Asam, S., Kuenzer, C., Dech, S., 2019. The effect of droughts on vegetation condition in Germany: an analysis based on two decades of satellite earth observation time series and crop yield statistics. Remote Sens. 11 (15), 1783.

Rodríguez-Iturbe, I., Rinaldo, A., 2001. Fractal River Basins: Chance and Self-Organization. Cambridge University Press, Cambridge, UK.

Rutherford Christopher, J., Young, G.R., G., R., Quinn, J.M., Chapra, S.C., Wilcock, R.J., 2020. Nutrient attenuation in streams: a simplified model to explain field observations. J. Environ. Eng. 146 (8), 04020092.

Schöl, A., Kirchesch, V., Bergfeld, T., Müller, D., 1999. Model-based analysis of oxygen budget and biological processes in the regulated rivers Moselle and Saar: modelling the influence of benthic filter feeders on phytoplankton. Hydrobiologia 410 (0), 167–176.

Sharma, D., Kansal, A., 2013. Assessment of river quality models: a review. Rev. Environ. Sci. Biotechnol. 12 (3), 285–311.

SKUMS (2019). *Pelagic chlorophyll-a monitoring data.* The free hanseatic city of bremen: senate of climate protection, environment, mobility, urban development and housing (SKUMS), https://www.bauumwelt.bremen.de/umwelt/wasser/oberflaechengewaesser/messstation_bremen_hemelingen-28654.

Soro, M.-P., Yao, K.M., Kouassi, N.L.B., Ouattara, A.A., Diaco, T, 2020. Modeling the Spatio-Temporal Evolution of Chlorophyll-A in Three Tropical Rivers Comoé. Bandama, and Bia Rivers (Côte d'Ivoire) by artificial neural network. Wetlands.

Stevenson, R.J., Smol, J.P., 2015. Chapter 21 - use of algae in ecological assessments. In: Wehr, J.D., Sheath, R.G., Kociolek, J.P. (Eds.), Freshwater Algae of North America. Academic Press, Boston, pp. 921–962.

Strahler, A.N., 1957. Quantitative analysis of watershed geomorphology. Eos Trans. AGU 38 (6), 913–920.

UNEP/JRC. (2019). *World water quality alliance.* Retrieved from https://www.unenvironment.org/news-and-stories/press-release/world-water-quality-alliance-launched-tackle-global-water-crisis.

Vannote, R.L., Minshall, G.W., Cummins, K.W., Sedell, J.R., Cushing, C.E., 1980. The river continuum concept. Can. J. Fish. Aquat. Sci. 37 (1), 130–137.

Wellen, C., Kamran-Disfani, A.-R., Arhonditsis, G.B., 2015. Evaluation of the current state of distributed watershed nutrient water quality modeling. Environ. Sci. Technol. 49 (6), 3278–3290.

Xia, R., Wang, G., Zhang, Y., Yang, P., Yang, Z., Ding, S., Jia, X., Yang, C., Liu, C., Ma, S., Lin, J., Wang, X., Hou, X., Zhang, K., Gao, X., Duan, P., Qian, C., 2020. River algal blooms are well predicted by antecedent environmental conditions. Water Res. 185, 116221.

Yang, S., Büttner, O., Jawitz, W.J., Kumar, R., Rao, P.S.C., Borchardt, D, 2019a. Spatial organization of human population and wastewater treatment plants in urbanized river basins. Water Resour. Res. 55 (7), 6138–6152.

Yang, S., Büttner, O., Kumar, R., Jäger, C.G., Jawitz, J.W., Rao, P.S.C., Borchardt, D, 2019b. Spatial patterns of water quality impairments from point source nutrient loads in Germany's largest national River Basin (Weser River). Sci. Total Environ. 697, 134145.

Yang, S., Paik, K., 2017. New findings on river network organization: law of eigenarea and relationships among hortonian scaling ratios. Fractals 25 (03), 1750029.

Zink, M., Kumar, R., Cuntz, M., Samaniego, L., 2017. A high-resolution dataset of water fluxes and states for Germany accounting for parametric uncertainty. Hydrol. Earth Syst. Sci. 21 (3), 1769–1790.